CFD simulation of Electrostatic Precipitators and Fabric Filters State of the Art and Applications

M. Feldkamp, M. Dickamp, C. Moser *

(ENVIROSERV GmbH, Essen, Germany * E-mail: Christian_Moser@envrioserv.de)

Abstract: This paper clearly discloses the possibilities, which the numeric flow simulation offers in case of modelling the two-phase flow in electrostatic precipitators and fabric filters with view to design new and retrofitting of old plants today. Contrary to physical flow models the CFD simulation is capable to consider high dust loads and the distribution of dust in the gas flow. This is an advantage which will lead to the displacement of the physical flow models by sophisticated CFD simulations while investigating the two phase flow in dust precipitators. This paper explains the main features of the used CFD models for the detailed simulation of these types of precipitators. Both CFD model approaches are based on an EULER-LAGRANGE formulation of the two-phase flow consisting of gas and solid particles. Also the paper points out, how important a highly detailed geometry model is for a strong simulation and reliable results. So all the ducts up- and downstream the precipitator itself including every inner part (e.g. guide vanes, dampers, etc.) are integrated in the CFD geometry model. The simulations show that today reliable CFD simulations of both precipitator types the electrostatic and the fabric filter in consideration of the phase interaction between gas and solid particles including separation are possible with high accuracy. Thus it is possible to examine special questions such as optimization of gas flow, reduction of pressure loss or the increase in separation efficiency, purposefully tailored to a precipitator, fast and economically.

Keywords: ESP, CFD, EHD, Geometry model

1 INTRODUCTION

For flue gas cleaning downstream of fossil fuel fired power plants or waste incineration plants dust precipitation has always been an essential process step. Since the requirements concerning dust emissions of power and incineration plants become more and more strictly, the design of filtering devices - either electrostatic precipitators or fabric filters – is getting more and more into focus in order to achieve maximum dedusting efficiency at minimized operating expenses. Not only the design of new filters is of interested but also the retrofit of existing filters is an important field of activity.

Computational Fluid Dynamics (CFD) has become an acknowledged tool for modelling the two phase flow – gas and washing liquid droplets – in wet flue gas desulphurisation (FGD) scrubbers, behind lignite or hard coal fired power plants, and has completely replaced the physical models. ENVIROSERV's CFD experts have long-term experience simulating two phase flow of FGD scrubbers including mass transfer of the air pollutant sulphur dioxide (SO_2) and have validated their applied models at various large scales FGD plants.

Based on that experience, ENVIROSERV conducts three-dimensional flow simulations of the two phase flow – gas and solid dust particles – of electrostatic precipitators and fabric filters, in order to improve the fluidic boundary conditions of the filter devices. Potential for optimisation offers the fluid dynamics, which was highly simplified during dimensioning so far. Particularly the incoming flow towards the electrostatic precipitators or the fabric filters is often very inhomogeneous with regard to velocity of gas and distribution of particles which leads to degradation of the precipitation efficiency.

Starting point for optimisation is the three-dimensional flow simulation of the gas flow in such a deduster with help of suitable and durable CFD simulations. Therefore the commercial software ANSYS CFX°11 is used to simulate the two-phase flow of gas and solid particles. The simulation of the two-phase flow itself is based on an EULER-LAGRANGE formulation, whereby gas and solid phase are two-way-coupled. Also all relevant boundary conditions – e.g. geometry, particle size distribution, electric field etc. – are implemented to the CFD software. For ESPs also the electro-hydrodynamic flow induced by the electric field is taken into account.

The paper outlines the fundamentals of CFD modelling of the two different types of dedusters (electrostatic precipitators and fabric filters) as well as examples from various plants applying the CFD simulation for optimisation of dedusters. The aim is to point out optimisation potential and possibilities, in order to increase precipitation efficiency and the performance in existing and new electrostatic precipitators and/or fabric filters. Furthermore the efficiency and the application possibilities of today's state of the art CFD simulations dealing with the two-phase flow, consisting of flue-gas and solid particles, are shown.

2 SIMULATION OF ELECTROSTATIC PRECIPITATORS

The use of electrostatic forces to separate fine particles from gases has been known and employed for many decades. The process, known as electrostatic precipitation, was first applied commercially in 1907 by Fredrick G. Cottrell. Since that time, electrostatic precipitators have been developed into efficient devices and play a major role in modern industrial particulate matter control. Nowadays electrostatic precipitators are widely applied in power stations and many other large-scale industrial systems in order to reduce fly ash and fine particles emissions by charging the particles in a corona discharge and separating them from the gas by means of an electric field.

Despite a general understanding of ESP operation and its successful use in industry, many questions regarding particle precipitation remain unanswered. This is not surprising since there is a very complex network of mechanisms that affect particle transport inside a precipitator. These phenomena are probably best understood as a strong interactive coupling of fluid dynamics, electrostatics, and particle dynamics. The existence of momentum coupling between the electrostatic field and fluid dynamic field give rise to a feature known as the electrohydrodynamics (EHD). Resulting from corona-generated ions that collide at high velocity with neutral gas molecules located between the discharge electrode and collecting plate, the electrohydrodynamic flow field is formed. The effect of this ionic wind on the gas flow field and the resulting impact on particle transport are possibly relevant to all the phenomena that occur within an ESP.

To investigate the characteristics of electrohydrodynamic gas flow as well as its effect on the particle precipitation, ENVIROSERV has developed a detailed CFD model to predict the motion of ions, gas and particles in an ESP. In this model the effect of ionic wind on the gas flow as well as the induced turbulence is examined. Furthermore, the particle motion is simulated, as mentioned before, by means of LAGRANGIAN approach. The precipitation efficiency of an ESP for particles is computed to understand how the EHD gas flow affects the particle precipitation.

3 ELECTROHYDRODYNAMICS (EHD)

The interaction of electrodynamics and hydrodynamics is often named electrohydrodynamics (EHD) and appears whenever a dielectric fluid is moving in an electric field. The dielectric fluid is characterized by a very small electrical conductivity, which give rise to only small currents even when an intense electric field is present. As a result, magnetic effects are negligible.

In an ESP, the fluid consists of neutral gas molecules and ions produced by the corona discharge. These ions drift mainly along the electric field lines. Due to collisions with neutral gas molecules, there is a momentum transfer to the flow by the electric field. The momentum imparted to the gas by the ion flux produces a highly directional gas flow toward the plate in the case of no primary flow. Due to continuity gas have to return to the corona region, thereby a recirculating flow is promoted. The resulting flow is called electrohydrodynamic flow or secondary flow.

Primary flow interacts with the secondary flow to produce a highly complex fluid dynamic field. According to many experimental works a positive corona discharge produces secondary flow in both horizontal and vertical planes as shown in Fig. 1, whereas for negative corona the secondary flow is more complicate, because an unsteady tuft-like discharge structure generates extra turbulence throughout the precipitator in comparison with the case of positive corona. These results indicate that the EHD flow is strongly dependent on corona polarity and precipitator inlet velocity.

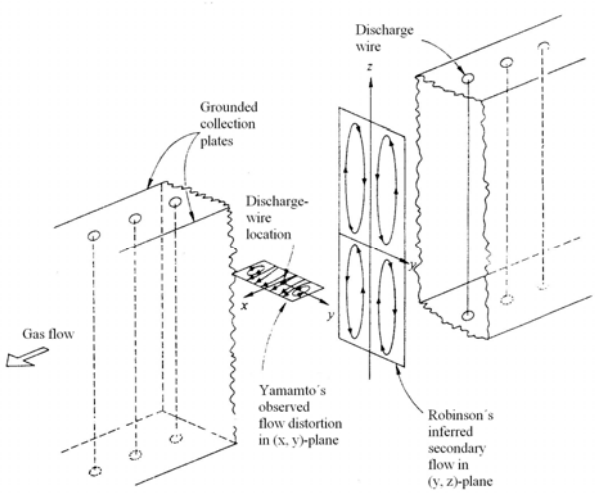

Fig. 1 The secondary-flow patterns observed by Robinson and Yamamoto in wire-plate precipitators

4 MODELLING

Electrostatic precipitation is characterized by the complex interaction of an electric field generated by corona discharge, a gas flow field and the particulate dynamics. The three physical sub-systems are coupled with each other as is shown in Fig. 2. Each physical phenomenon is certainly influenced by the equipment geometry, especially the size and shape of the discharge and precipitation electrode. For the methodical modelling, a modular approach in which each sub-system is respectively modelled is required. The aim is to link the above mentioned three sub-systems at last and form a complete method for modelling an electrostatic precipitator. In order to simplify the physical phenomena, we assume that the material properties are constants and the gas flow is steady as well as incompressible. The entire process is isotherm so that the heat transfer is ignored.

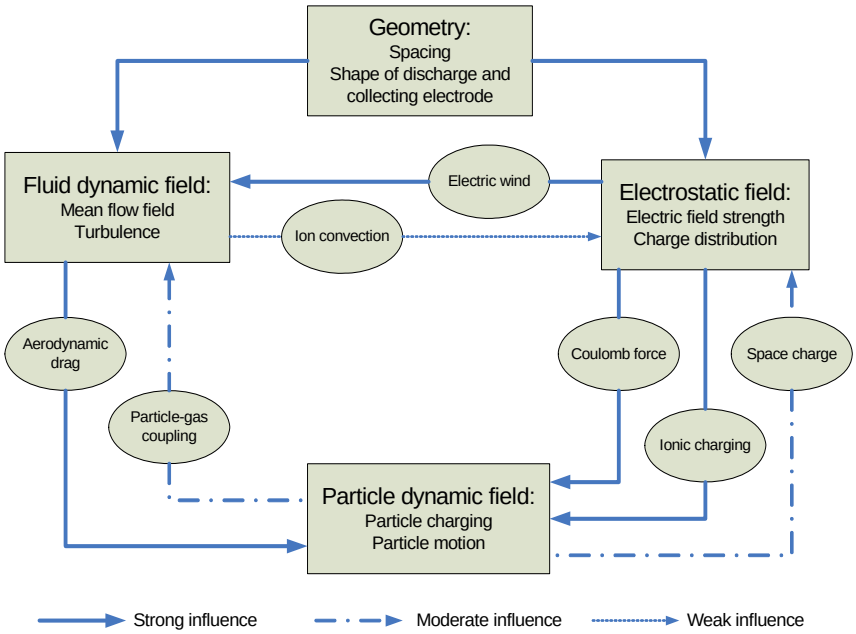

Fig. 2 Interaction of different physical phenomena in electrostatic precipitators

At last it can be summarized that the following governing equations are essential for the modelling of EHD flow and the corresponding particle motion in an ESP.

1. Poisson equation:

$$\nabla^2\phi = -\frac{\rho_{ion}}{\varepsilon_0}$$

2. Conservation of space charge density:

$$\nabla\cdot(\rho_{ion}b_{ion}\vec{E} + \rho_{ion}\vec{u} - D_{ion}\nabla\rho_{ion}) = 0$$

3. Electric field – Electric potential relation:

$$\vec{E} = -\nabla\phi$$

4. Continuity of gas flow:

$$\nabla\cdot\vec{u} = 0$$

5. Conservation of momentum:

$$\vec{u}\cdot\nabla\vec{u} = -\frac{\nabla P}{\rho} + (\mu+\mu_t)\nabla^2\vec{u} + \rho_{ion}\vec{E}$$

6. Equation of particle motion:

$$m_p\frac{d\vec{u}_{p_i}}{dt} = \frac{1}{2}C_D\rho A\left|\vec{u}_{fi} - \vec{u}_{p_i}\right|(\vec{u}_{fi} - \vec{u}_{p_i}) + m_p\frac{g(\rho_p-\rho)}{\rho_p} + q_p\vec{E}_i$$

4 VALIDATING

The investigation of the EHD flow in an ESP works on the premise that the electric field should be simulated accurately. Therefore a validation of the MHD modelling approach discussed before is essential. This section will discuss the relevant simulation of the electric field. It includes that the perdition results are compared with measured data found in literature.

The often-quoted experimental results of Penney and Matick was one selected option to validate the model. The precipitator used in Penney and Matick experimental work was arranged with a simple wire-plate system which contained four wires.

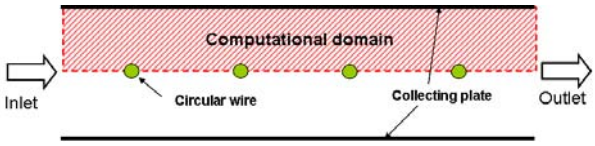

Fig. 3 Precipitator in Penney and Matick experimental work

It has been carried out with a combination of two different wire diameters and three settings of corona voltage. The geometric and operation data of their work is summarized in Table 1.

Table 1 Geometric and operation data of the examined cases

Case No.	Wire radius (mm)	Wire to plate space (mm)	Wire to wire space (mm)	Voltage (kV)
1	0.1524	114.3	152.4	25.5; 43.5
2	1.016			38.7; 43.5; 46.2

In order to decrease simulation time, a single wire geometry with a length that equals the wire to wire space in a four-wires precipitator is used as computational domain. Fig. 4 shows an example of ion charge distribution for no cross flow with the geometric and operation data used in the Penney and Matick's experimental study.

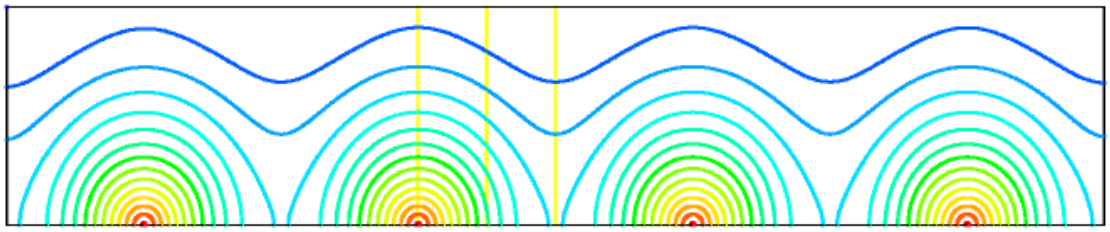

Fig. 4 An example of ion charge distribution in a four-wires precipitator

It is seen that the electric conditions around each wire are completely identical. In the experimental study, electric potentials are measured along three yellow lines as shown in Fig. 4. To clarify the concrete location in the comparison between experimental data and prediction, line 1, 2 and 3 are used in the following discussion.

Fig. 5 compares the computed voltage distribution at line 1, 2, 3 with the experimental data of Penney and Matick. The result on the case 1 (r_{wire} = 0.1524 mm) shows that the model prediction by using method 1 is in a very good agreement with the experimental data.

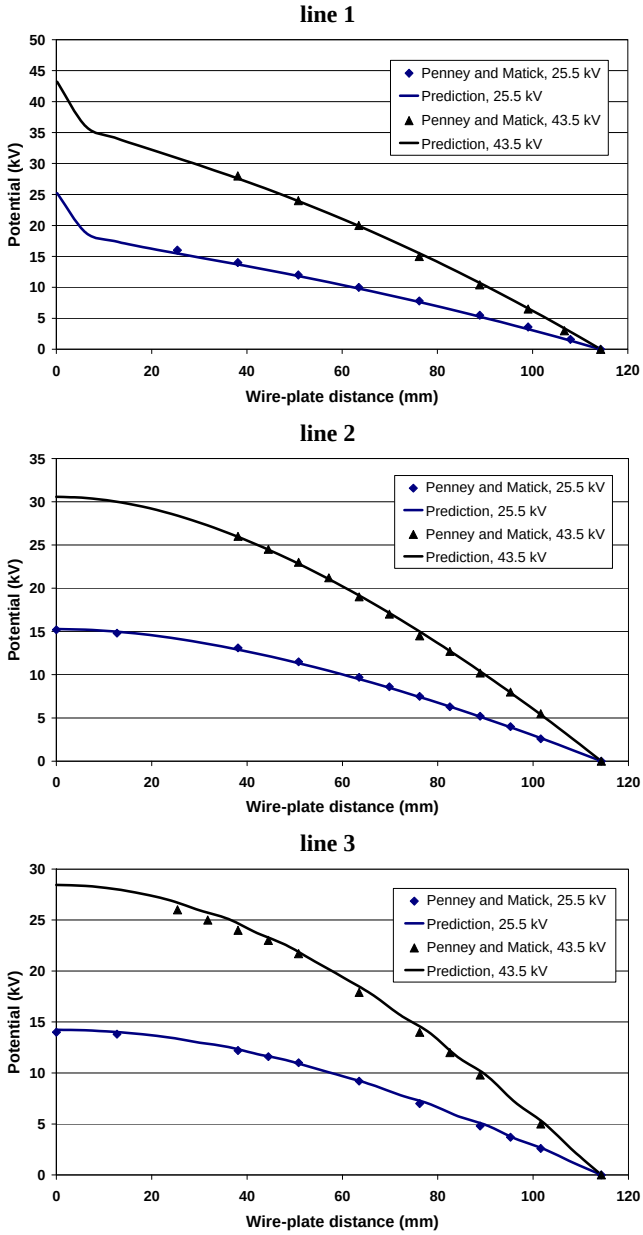

Fig. 5 Comparison of the predicted potential variation with the measurements of Penney and Matick (r_{wire} = 0.1524 mm)

To show the effect of cross flow velocity on the electric field, a series of simulations with inlet velocity 0 m/s, 0.5 m/s, 1 m/s and 3 m/s are executed. The flow direction is from left to right.

Fig. 6 shows the ion charge density distribution in the one-wire precipitator with different inlet velocities of 0 m/s and 3 m/s. The ion charge distribution in the case of no cross flow is symmetric. However, as the cross-flow inlet velocity increases, the contours of ion charge density become asymmetric. The gas flow sweeps the ions to the downstream region of the wire. As a result, the ion charge density in the downstream region of corona wire is larger than that on the upstream side.

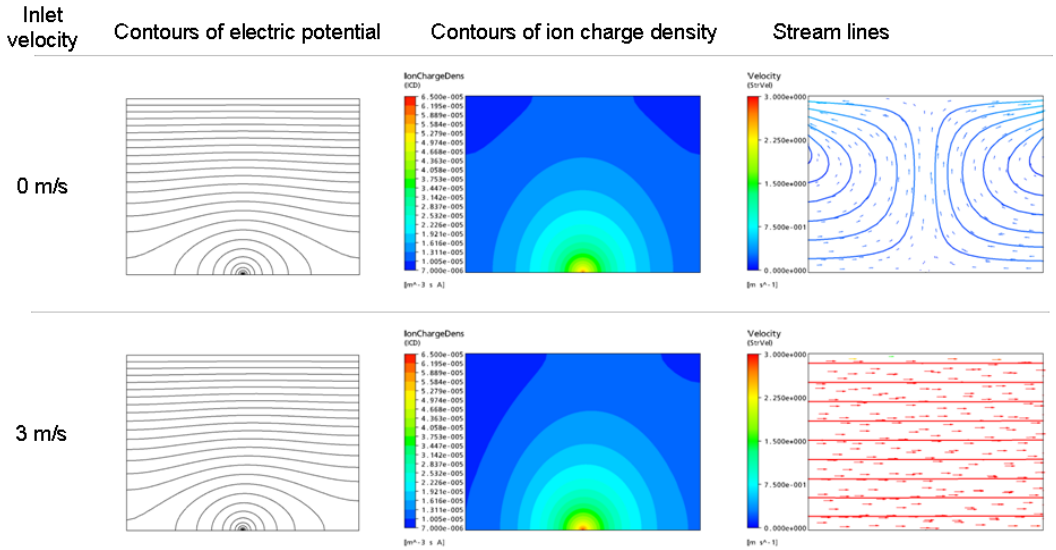

Fig. 6 Ion charge density contours for different cross flow velocities

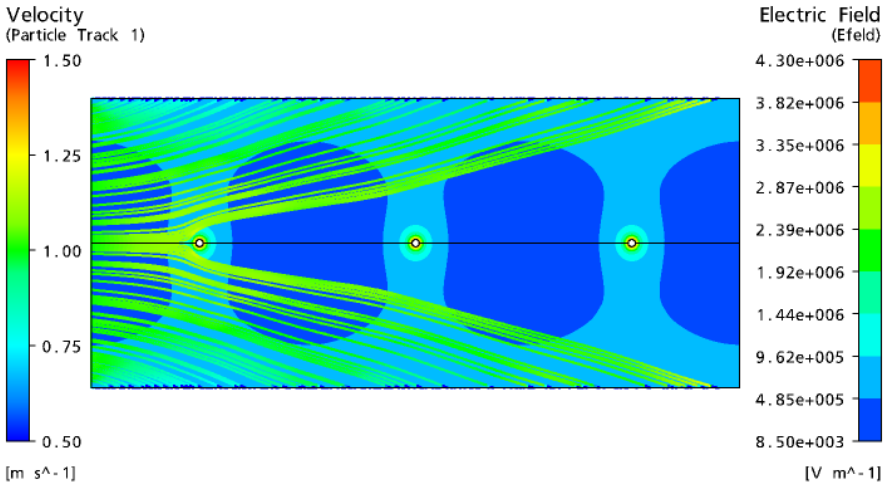

Fig. 7 Particle trajectory and electric field contour

After testing and validating these fundamental electrohydrodynamic model parameters, the next step was to simulate solid particles in these EHD simulations as well. Fig. 7 shows the particle path for the operating conditions. The simulation is accomplished using medium turbulence intensity at the inlet. In the shown test case 400 particles with same diameter are simulated. The particles are assumed as trapped once they touch the ground plate.

5 SIMULATION AND OPTIMISATION OF AN INSTALLED ESP

After validation the model approach, as it was discussed before, the simulation of a real ESP is now possible. In the following part of this paper some simulation results of a real ESP will be shown in detail. The ESP, shown in Fig. 8, is located behind four lignite fired boilers. In this case the duct system towards the ESP has to be retrofitted and the goal was to achieve a homogenous gas velocity flow towards the ESP, to get an optimized efficiency.

Fig. 8 ESP before retrofitting

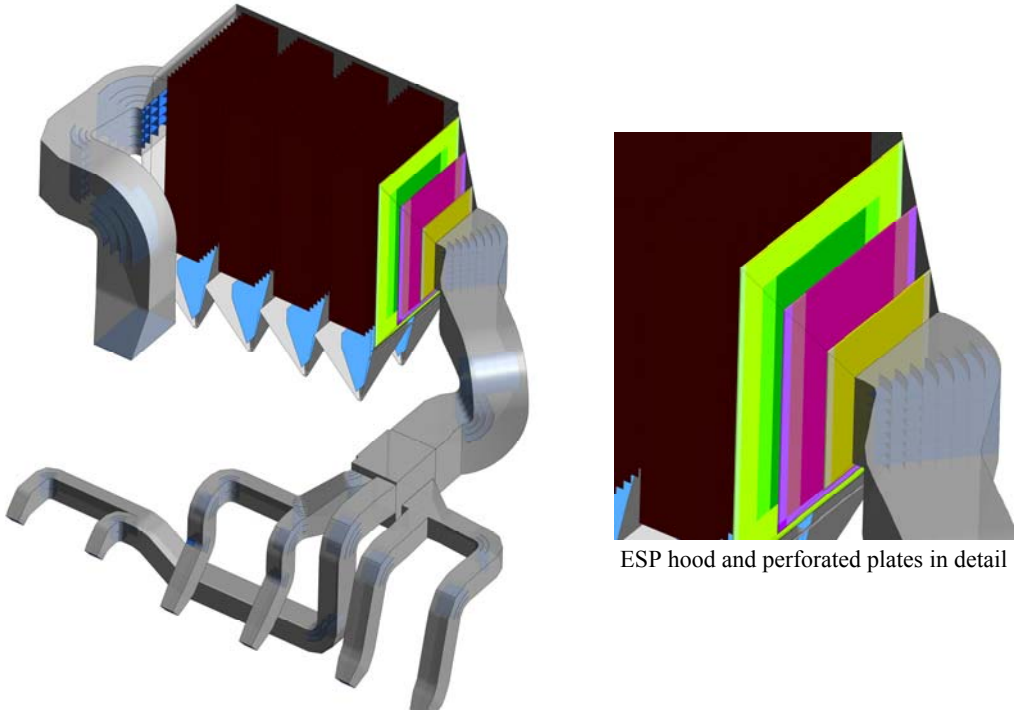

ESP hood and perforated plates in detail

Fig. 9 CFD model of the retrofitted ESP

The ESP and the incoming and leaving ductwork were transformed into a very detailed CFD model, which is show for the retrofitted, optimized case in Fig. 9.

In the above Fig. 9 it can be seen that all ductwork is been simulated. This is necessary to get the correct velocity distribution at the inlet of the ESP (see Fig. 10) hood and, as result of that, the right gas/solid flow through the ESP itself. On the other side this is the only way to include the upstream guide vanes into the CFD model, which can not be neglected in the optimisation process.

The results of the optimisation, concerning the homogenisation of the gas velocity distribution, are shown in Fig. 10 for the ESP inlet hood.

Fig. 10 displays the velocity distribution on different planes normal to the gas flow direction over the ESP inlet hood (see also Fig. 9). That means the displayed planes are at the inlet of the ESP hood, at the three perforated plates and on the plane leaving the hood.

As expected, the average axial gas velocity decreases from the inlet of the ESP hood towards to the inlet of the ESP chamber from 15.95 m/s to 1.63 m/s, according to the increasing cross section of the hood/cut planes.

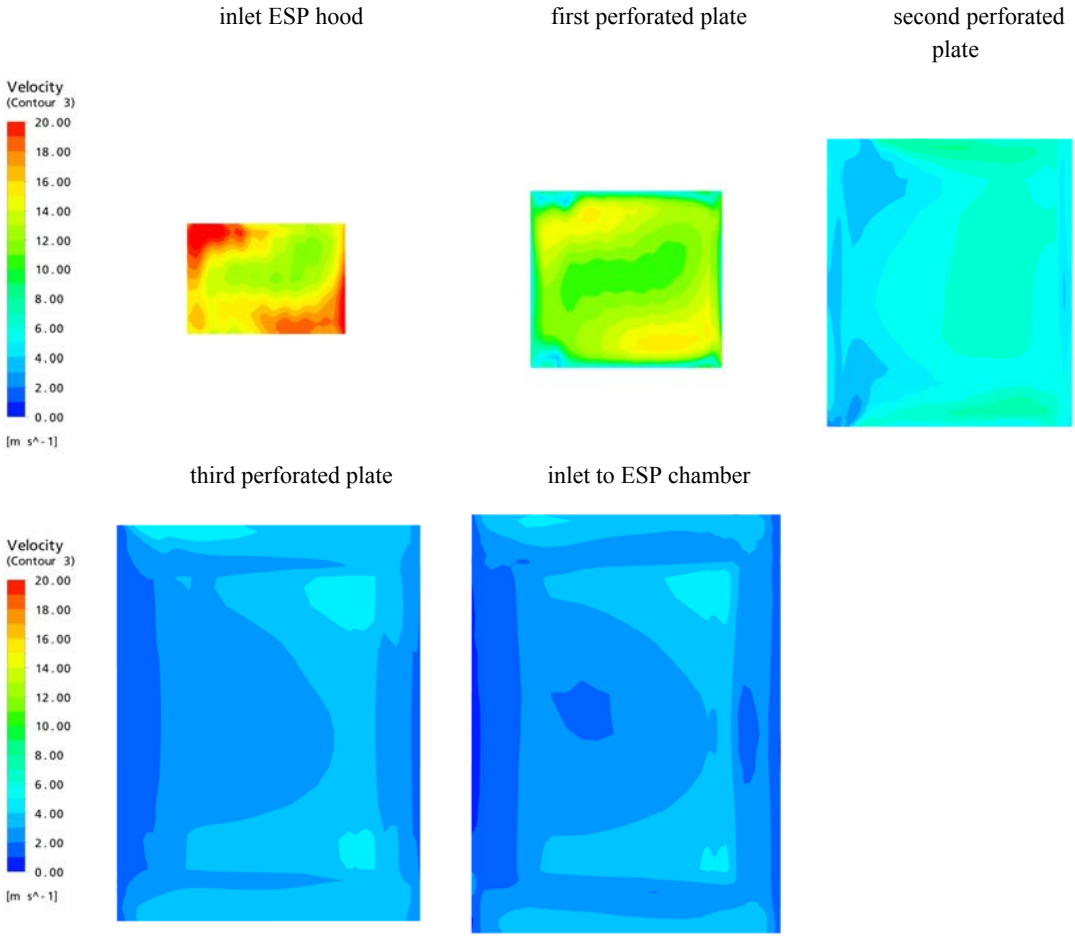

Fig. 10 Velocity distribution over the ESP inlet hood

Table 2 Geometric and operation data of the examined cases

	axial gas velocity [m/s]			
	max	min	average	□
inlet ESP hood	22.15	6.26	15.95	2.62
first perforated plate	13.49	0.33	5.48	3.49
second perforated plate	6.13	1.29	3.43	0.90
third perforated plate	3.64	0.71	1.85	0.69
inlet to ESP chamber	3.58	0.42	1.63	0.69

Simultaneously the standard deviation of the axial gas velocity, as quantity for the uniformity and homogeneousness of the gas flow, decreases, too. The exact values oft the axial gas velocity on the cut planes according to Fig. 10 are given in Table 2. This is a result of optimising the perforated plates with the help of the CFD simulation model discussed in detail before.

Also the velocity distribution on a horizontal cut through the ESP, which is show in Fig. 11, points out the uniformity of the gas flow as a result of the optimisation.

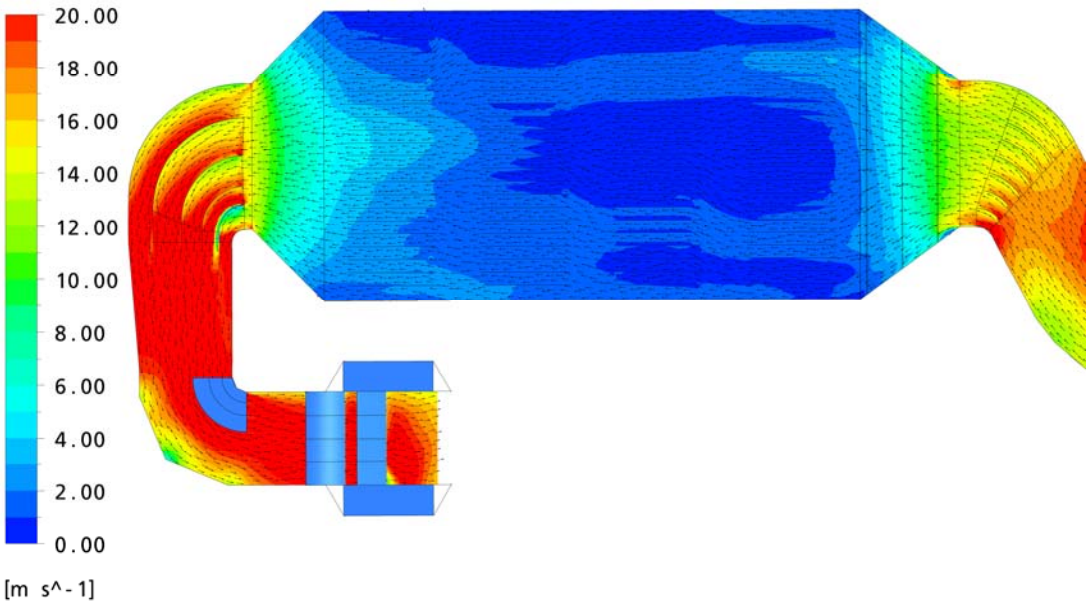

Fig. 11 Velocity distribution inside ESP

6 SIMULATION OF FABRIC FILTERS

The simulation of fabric filters is based on Euler-Lagrange approach, too. Therefore the basic conservation equations are the same as in the model for electrostatic precipitators described before. Also in this model the force balance around the solid particles is used to describe the solid particle motion. This goes back to ENVIROSERVs long term experience with the wet two-phase FGD scrubber simulation model, where a gas flow with fluid particles (droplets) is handled. But in opposite to the simulation of electrostatic precipitators there is no need for a MHD model.

But it is important to model the filter elements in detail in this model. First this means that the pressure loss of the filter elements has to be taken into account. The pressure loss is implemented according to DARCYs law for a porous medium. The general form of DARCYs law for a single component i of the gas is:

$$\frac{\partial p}{\partial x_i} = -\frac{\mu_G}{K_{perm}} U_i - K_{loss} \rho_G |\boldsymbol{U}| U_i$$

Secondly the precipitation of the solid particles at the filter elements has to be modelled. Here a separation curve based on the particle diameter and the particle velocity is integrated.

7 SIMULATION AND OPTIMISATION OF AN INSTALLED FABRIC FILTER

This part of the paper should show some results of the simulation of an installed fabric filter with the ENVIROSERV CFD model. The fabric filter, shown in Fig. 12, is part of a Circulating Fluidised Bed (CFB) Flue Gas Desulphurisation (FGD) plant. The outlet dust concentration downstream the CFB FGD is up to 1000 g/m^3 which requires a very uniform dust distribution to all chambers of the fabric filter.

In this case again the duct system towards the fabric filter is modelled in detail to get the correct gas flow towards the fabric filter and the filter elements.

Fig. 12 Real filter

Fig. 13 show the 3D geometry model that is used for simulation. The grid for the numerical calculation of this fabric filter consists of structured and unstructured parts and has a size of 12 Mio. elements.

One highlight is the detailed exposition of each single filter element in this CFD geometry model (see Fig. 14). Again and that had to keep in mind, all inner parts (e.g. guide vanes) inside the ducts are taken into account and component part of the geometry model.

One result of the simulation is the gas velocity distribution in the filter. In this paper only the gas velocity at some specific areas should be discussed.

Fig. 15 shows the gas velocity on a vertical cut plane through the filter. The raw gas side can be found on the left side (higher gas velocities) and the clean gas side is on the right side (lower gas velocities).

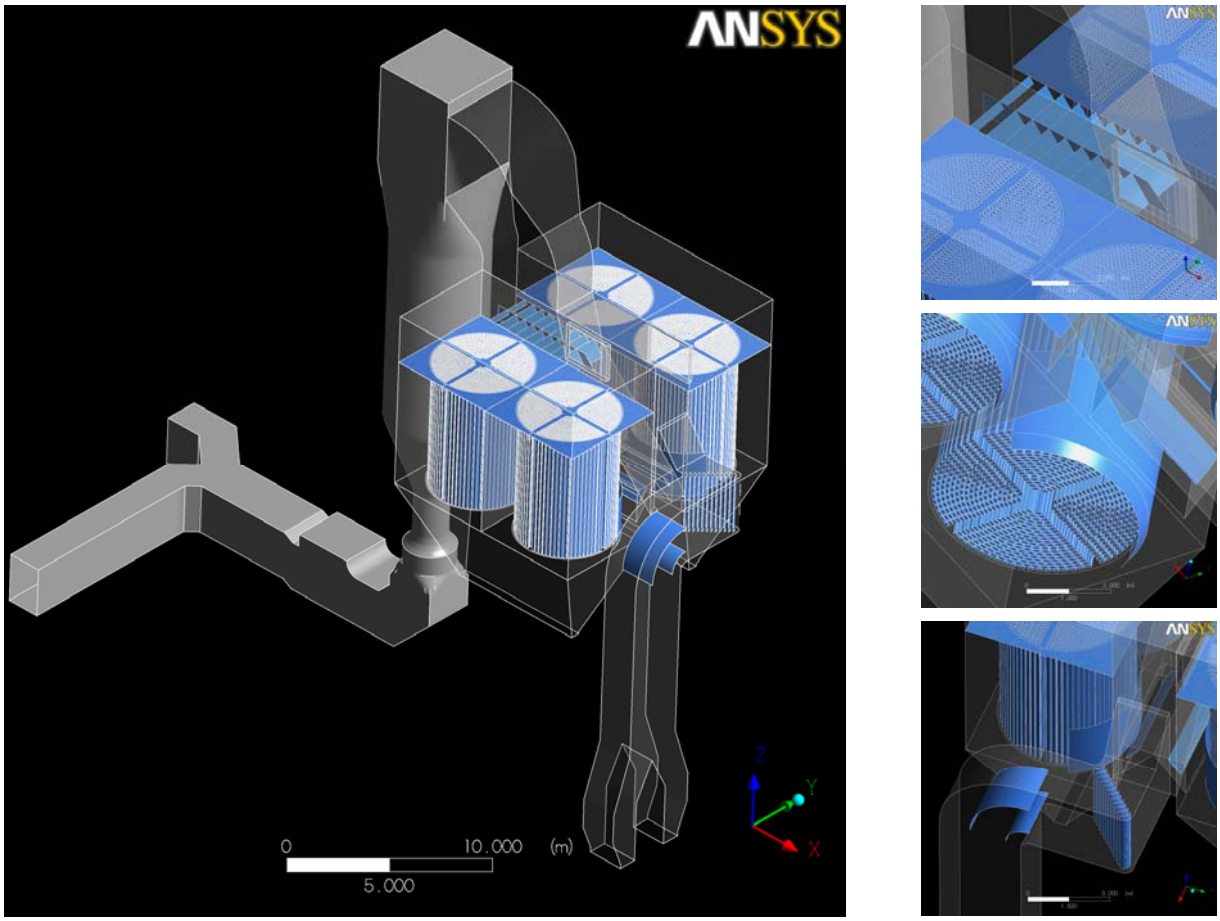

Fig. 13 Detailed 3D CFD model of the Filter including all inner parts

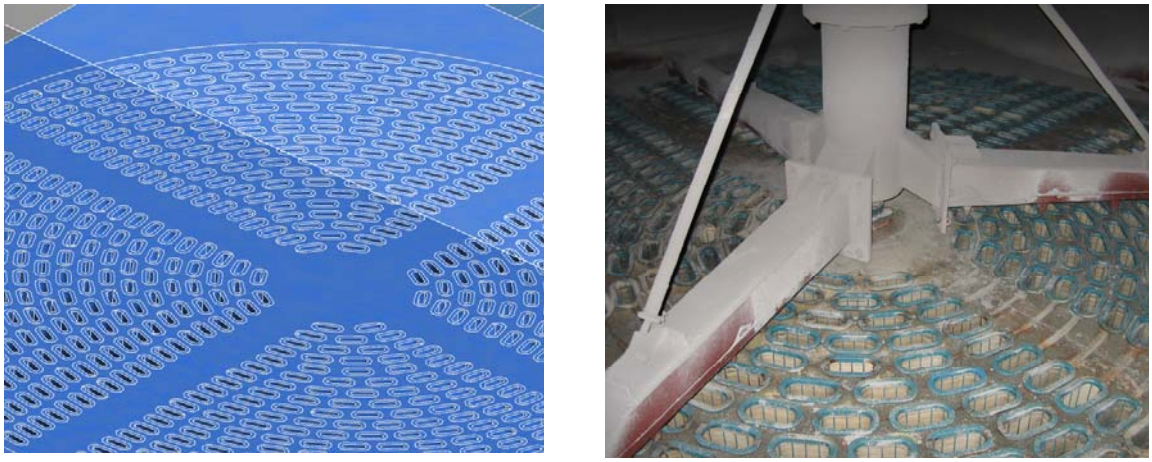

Fig. 14 filter elements in CFD model and reality

Also the position of the guide vanes in the raw gas part of the filter can be found easily. So that it is now possible to optimise these guide vanes to unify the gas flow towards the filter chambers and the filter elements.

The flow field towards the single filter elements can also be watched and optimised through the presented CFD model. As the next Fig. 16 shows (on horizontal a cut plane), it is possible with this CFD tool to make the gas velocity distribution around every single filter element visible in a short period of time.

Therefore optimisations regarding the filter chambers and the filter elements are now well directed possible.

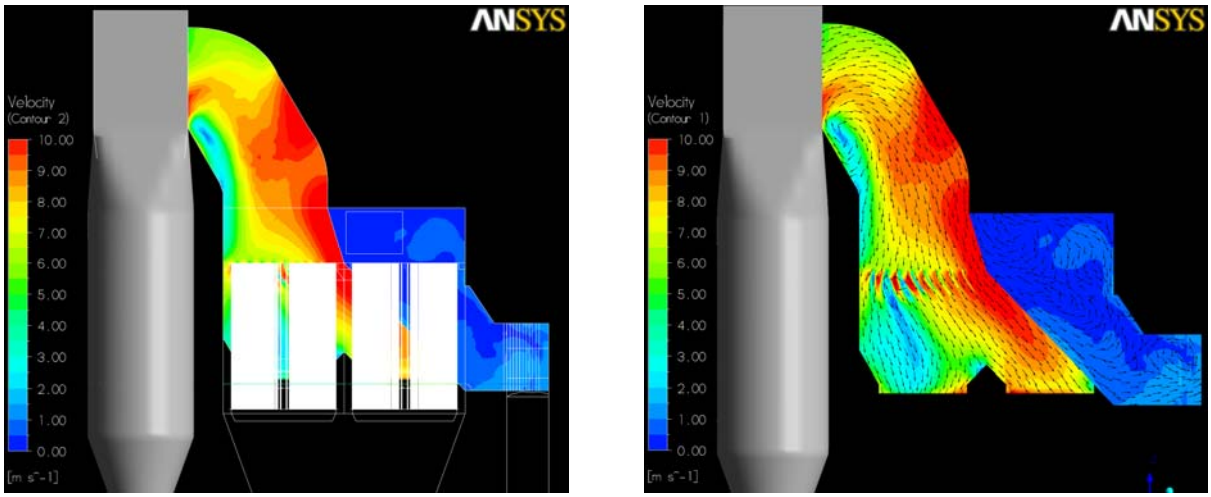

Fig. 15 Gas velocity on vertical cut through filter

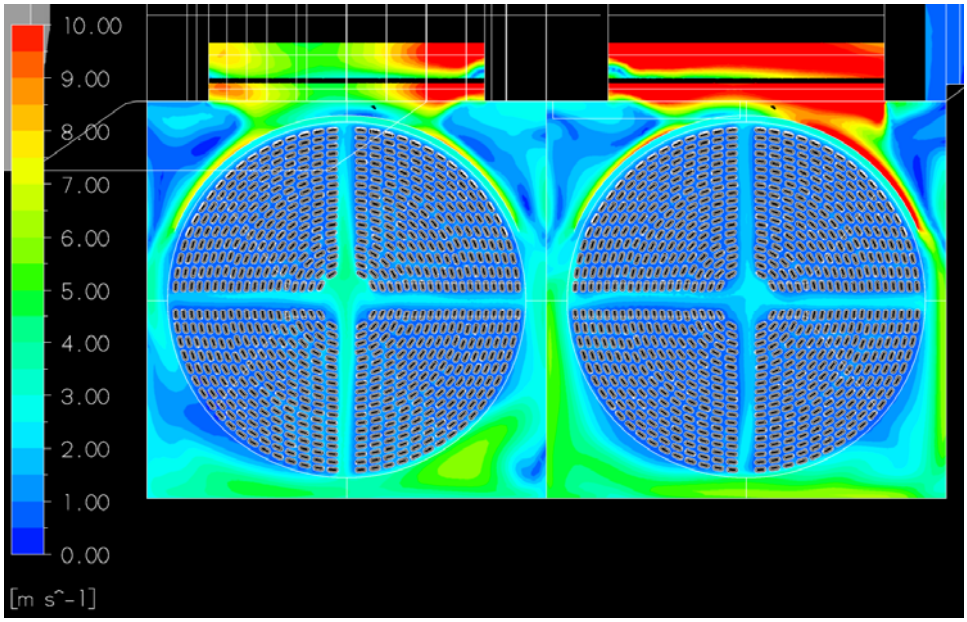

Fig. 16 Gas velocity distribution around filter elements